

Slow Crack Propagation and Slip Correlations

J. SCHMITTBUHL,¹ A. DELAPLACE,² K. J. MÅLØY,³
H. PERFETTINI,⁴ and J. P. VILOTTE⁵

Abstract—The propagation of an interfacial crack through a weak plane of a transparent Plexiglas block is studied experimentally. The toughness is controlled artificially by a sand blasting procedure, and fluctuates locally in space like uncorrelated random noise. The block is fractured in mode I at low speed ($10^{-7} - 10^{-4}$ m/s). The crack front is observed optically with a microscope and a high resolution digital camera. During the propagation, the front is pinned by micro-regions of high toughness and becomes rough. Roughness of the crack front is analyzed in terms of self-affinity. The in-plane roughness exponent is shown to be 0.63 ± 0.05 . Experimental results are compared to a numerical model. The model reproduces the self-affine behavior of the crack front, i.e., long-range correlations of the roughness. Analogies between mode I and mode III are presented in order to discuss implications of the experimental results for creeping faults. Accordingly, correlations of the slip pattern are shown to exist over scales substantially larger than the asperity sizes.

Key words: ■

1. Introduction

The propagation of rupture front through heterogeneous solids is a central question for numerous mechanical problems. One main evidence of the fluctuating front propagation is the roughness of fracture surfaces. Numerous works have shown the self-affine properties of crack surfaces (BROWN and SCHOLZ, 1985; BOUCHAUD *et al.*, 1990; MÅLØY *et al.*, 1992; COX and WANG, 1993; SCHMITTBUHL *et al.*, 1995b; BOUCHAUD, 1997). The out-plane roughness exponent ($\zeta \approx 0.80$) is found to be very robust over different materials, different fracture modes and a broad range of length scales (BROWN and SCHOLZ, 1985; POWER *et al.*, 1987; SCHMITTBUHL *et al.*, 1993; SCHOLZ, 1990). A possible “universal” self-affine crack geometry of heterogeneous material has been proposed by BOUCHAUD *et al.*

¹ Laboratoire de Géologie, UMR 8538, Ecole Normale Supérieure, Paris, France.
E-mail: Jean.Schmittbuhl@ens.fr

² Laboratoire de Mécanique et Technologie, Ecole Normale Supérieure, Cachan, France.

³ Fysisk Institutt, Universitetet i Oslo, Oslo, Norway.

⁴ Laboratoire de Géophysique Interne et Tectonophysique, Grenoble, France.

⁵ Département de Sismologie, UMR 7580, Institut de Physique du Globe, Paris, France.



S B O 1 2 3 0 4
Journal number Manuscript number



Dispatch: 8.9.2002 Journal: Pure and applied Geophysics No. of pages: 16
Author's disk received Used Corrupted Mismatch Keyed

(1990). Studies of fracture surfaces and models of crack propagation are generally linked: the morphology of the crack surface is often assumed as inherited from the geometry of the crack front (BOUCHAUD *et al.*, 1993). Consequently, the mechanisms of the crack-front geometry during its propagation becomes a key question.

Even when the rupture front is interfacial, i.e., restricted to move within a plane (see Fig. 1), the motion results from interactions between non-local elastic coupling, inertia, wave effects, and quenched heterogeneities at different scales (PERRIN and RICE, 1994; RICE *et al.*, 1994; RAMANATHAN and FISHER, 1997; WILLIS and MOVCHAN, 1995; FISHER, 1998). The front is trapped temporarily by local asperities that may be related to local material heterogeneities or residual (i.e., internal) stresses. Depinning from these asperities involves local instabilities. When the elastic coupling is small, the motion is controlled by individual asperities. On the contrary for strong elastic coupling, asperities interact because of elasticity and the dynamics becomes global.

The aim of this paper is to discuss recent experimental results that describe the propagation of a tensile crack front along a heterogeneous weak plane, and to compare them to a simple numerical model. These results may be relevant for other modes of loading and shear fault rupture, at least for model elastodynamic theory that involves a single displacement variable. In particular, the dynamic spatial correlations may have interesting implications for creeping faults, as will be discussed briefly in the last section.

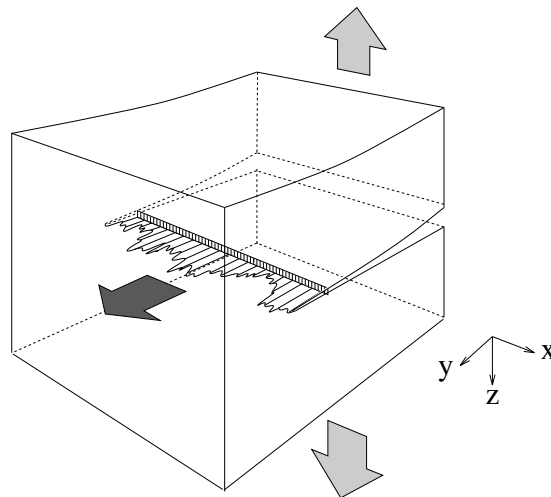


Figure 1

Sketch of the interfacial fracture crack propagation.

2. Experimental Setup

Samples are made of transparent polymethylmethacrylate (PMMA). Each PMMA sample is obtained from the assembling of two plates (SCHMITTBUHL and MÅLØY, 1997; DELAPLACE *et al.*, 1999). The upper plate is 32 cm \times 14 cm and 1 cm thick. The lower plate is 34 cm \times 12 cm wide and 0.4 cm thick. Each plate is sand-blasted on one side. One important consequence of the sand-blasting is that the transparency of the PMMA is lost, as light scatters from the introduced microstructures. The plates are then annealed together in an oven under a homogeneously normal pressure. The annealing procedure lasts 30 min at a temperature of 205 °C (see Fig. 2).

After annealing both plates together, the newly formed block recovers its transparency. New polymer chains are formed through the rough interface and air bubbles are extracted with the pressure load. The difference of the refraction index along the interfaces disappears. During the experiment, the plates are moved apart and a fracture propagates; the polymer chains within the weak plane are broken. The difference of refraction indexes across the interface is recovered and the fracture surface appears opaque due to the light scattering from the microstructures. The transition between the transparent and opaque regions corresponds to the crack front (see Fig. 3).

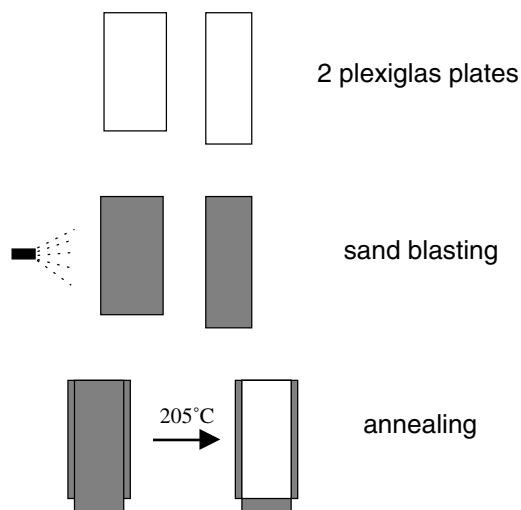


Figure 2

Sample preparation procedure. Two Plexiglas plates of 32 cm \times 14 cm and 34 cm \times 12 cm are cut and sintered together at 205 °C to form a single new block. Before the annealing process, both plates are sand-blasted with 50 μ m steel particles. Sandblasting creates roughness fluctuations that control the local toughness during sintering. Sandblasting also unpolishes the surfaces which induces a loss of transparency.

However, transparency is recovered during the sintering process.

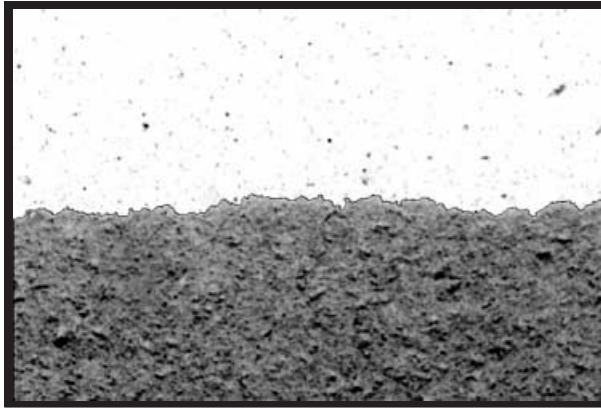


Figure 3

Example of a crack front picture using the Kodak DSC420 camera. The resolution is 1536×1024 pixels. The image covers an area of $6.5 \text{ mm} \times 4 \text{ mm}$. The crack is propagating from bottom to top. The cracked area is in dark gray. The front obtained from image treatment is superimposed as a black line.

Sandblasting roughens the surfaces of the PMMA plates. The magnitude of the roughness is less than a few micrometers. The random position of the defaults was checked optically using a microscope. Optical signatures of the flaws were observed to be smaller than a cutoff of about $50 \mu\text{m}$ corresponding to the size of the particle used for the blasting. The height fluctuations introduced by the sandblasting procedure introduce fluctuations in the toughness during the annealing process. We expect the toughness to be uncorrelated on length scales larger than the cutoff length. However, the correlation in the toughness up to this length scale is an open question.

At the final stage, one block with a weak annealing plane is obtained where the crack will propagate. The crack plane is referred as (x, y) : the y axis is along the crack propagation direction and the x axis is parallel to the mean crack front.

The thick plate of the PMMA block is clamped to a stiff aluminum frame. A normal displacement is imposed to the thin plate with a rod parallel to the crack front. By using an imposed displacement, we obtain a *stable* crack propagation in mode I. Oil is added to reduce friction between the thin plate and the rod. The rod is moved vertically by a continuous motor which allows a quasi-static loading. Typically the imposed displacement rate is slow: in the range $10^{-7} - 10^{-4} \text{ m/s}$.

The fracture propagates within the weak plane of the PMMA block. During the propagation, the front is pinned by local regions of high toughness and becomes rough. The geometry of the crack front is observed with a microscope. When static positions of the fronts are analyzed, a digital camera, set on the top of the microscope, provides high resolution images: 1536×1024 pixels. Each pixel covers a region of $2.6 \mu\text{m} \times 2.6 \mu\text{m}$. A sample picture is shown in Figure 4. In the inverted image, the sintered part is seen as light while the dark region represents the fracture

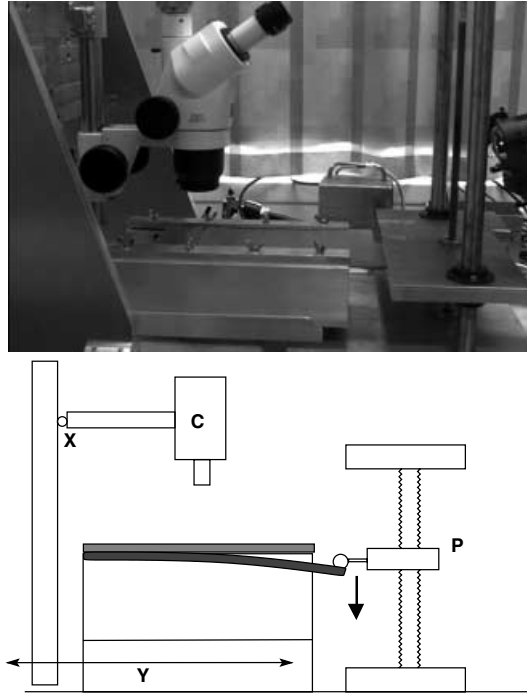


Figure 4

Picture and sketch of the experimental setup. The PMMA block made of two sintered plates is drawn with grays. The lower plate (dark gray) is bent thanks to a mechanical press (P) at constant displacement rate. The crack propagates in the y direction and is observed from above using a digital camera (C). The camera is attached to a moving frame that can be translated in both x and y directions.

aperture. The front is defined as the contrast boundary between the dark and the light areas and is found by using a specially developed software.

3. Roughness of Pinned Fronts

Measurements have been performed after a complete stop of the press when the crack front is at rest. The microscope is translated along the front (x direction) and up to 20 pictures of the front are taken. Neighboring pictures overlap one another over one third of the picture width (i.e., over 1.3 mm). Subfronts are extracted from each picture and averaged at overlapping positions. The assembling of 20 pictures provides a high resolution crack front, i.e., full front (up to 2^{14} data points) 45 mm long (see Fig. 5). A complete description of the assembling procedure can be found in (DELAPLACE *et al.* (1999)).

The in-plane roughness of the crack front is analyzed in terms of self-affinity. A self-affine front line $A(x)$ is statistically invariant under the scale transformation:

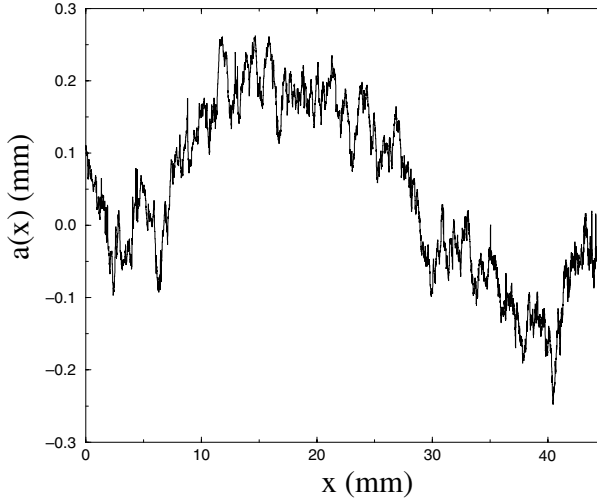


Figure 5

Sample of high resolution front obtained by assembling 20 pictures. Note that the vertical axis is magnified by a factor 75.

$(x, A) \rightarrow (\lambda x, \lambda^\zeta A)$ where ζ is the roughness exponent. Numerous techniques exist to probe the self-affine behavior and estimate the roughness exponent. Figure 6 presents an analysis based on a recent technique that uses a wavelet transform: The Average Wavelet Coefficient (AWC) technique (SIMONSEN *et al.*, 1998). A power-law behavior fits nicely the data both for the entire front and the subfronts, which shows the self-affine property of the crack front at rest. The expected slope for an artificial self-affine profile with a roughness exponent ζ is: $\zeta + 1/2(W(a) = \langle W_b(a) \rangle_b \propto a^{\zeta+1/2}$ where a is the scale factor of the wavelet and b the translation factor; an average is performed over the translation factor b). This provides an estimate of the roughness exponent of the crack front: $\zeta \approx 0.60$.

Results are consistent with the power spectrum analysis of the front roughness. Indeed, Figure 7 shows the power spectrum of the full front and the average over each individual subfront. The power-law behavior is also consistent with a self-affine property of the crack front. The slope of the spectrum for an artificial front with an exponent ζ is: $P(k) \propto k^{-2\zeta-1}$. From Figure 7, the roughness exponent of the crack front is also close to $\zeta \approx 0.60$.

In DELAPLACE *et al.* (1999) a full analysis of nine independent full fronts has been performed using four different techniques (SCHMITTBUHL *et al.*, 1995c): the variable bandwidth method, the multiple return probability method, the power spectrum analysis and the AWC method. All methods are consistent, and the final estimate of the roughness exponent is: $\zeta = 0.63 \pm 0.03$.

By performing the full analyses of the self-affinity property of the crack fronts, one observes that the scaling shows an upper cut-off that might be related to the

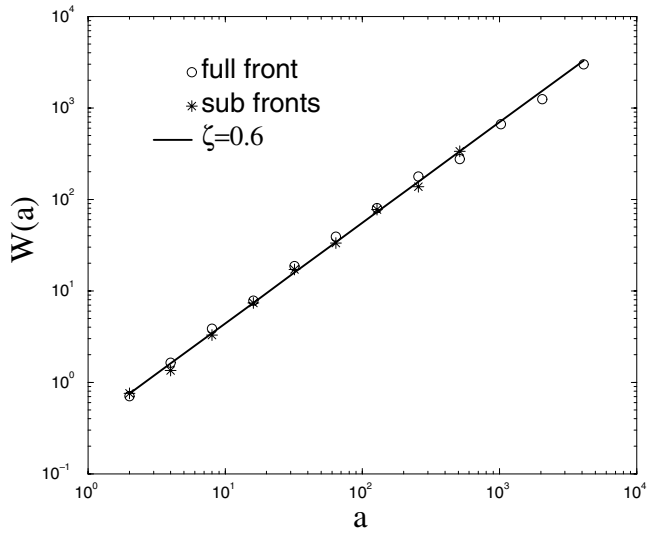


Figure 6

Self-affine analysis of a full-front (i.e., an assembled front from 20 pictures) using the Average Wavelet Coefficient method. The scale a is in pixel unit (i.e., $2.6 \mu\text{m}$). The average analysis of each individual subfront is superimposed in the figure. The log-log diagram shows a power-law behavior with a slope of 1.1, consistent with a roughness exponent of 0.6.

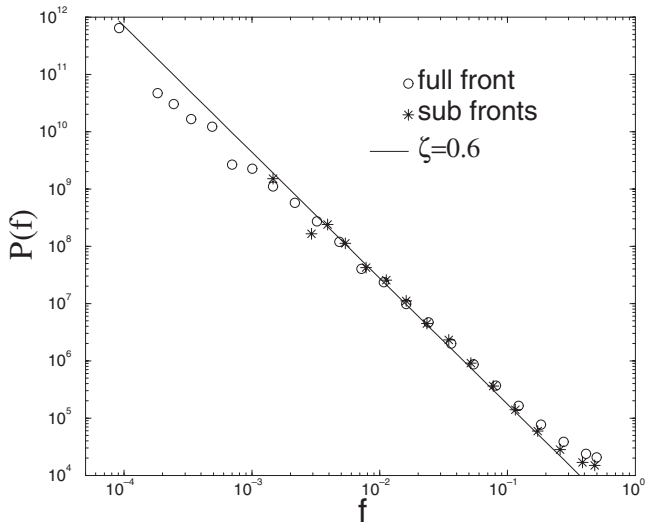


Figure 7

Self-affine analysis of a full-front (i.e., an assembled front from 20 pictures) using the Power Spectrum method. The wavelength unit is in pixel^{-1} where one pixel is $2.6 \mu\text{m}$ wide. The average analysis of each individual subfront is superimposed in the figure. The log-log diagram displays a power-law behavior with a slope of -2.2 , consistent with a roughness exponent of 0.6.

thickness of the Plexiglas plate. Further studies are ongoing for a careful check of the influence of the Plexiglas plate thickness.

4. A Mode I Crack Model

We assume that the roughness magnitude is always significantly smaller than the plate thickness. Accordingly, the experiment is modelled as a half-plane tensile crack propagating through an unbounded elastic solid. The crack is restricted to move in the plane $z = 0$, along the y direction. The crack front position, at time t , is described by a curve $y = A(x, t)$ that is assumed to be single-valued, excluding configurations with overhangs. To first-order, $A(x, t) = v_{cr}t + a(x, t)$ where v_{cr} is a uniform crack extension velocity and $a(x, t)$ the small amplitude deviation around that configuration with zero mean.

The energy per unit area of the interface that must be provided to fracture the solid is denoted $\Gamma(x, A(x, t))$. Interface heterogeneities are considered here as fluctuations in the local energy density: $\Gamma(x, y) = \Gamma_0[1 + \gamma(x, y)]$ where Γ_0 is the mean value of the interface fracture resistance and $\gamma(x, y)$ a dimensionless random quenched fluctuation of zero mean.

The analysis is restricted to a scalar approximation of elasticity (RICE *et al.*, 1994). The displacement field is then a scalar variable $u(x, y, z, t)$, and the associated tensile stress across planes parallel to the crack is $\sigma = (\lambda + 2\mu)(\partial u / \partial z)$, with λ and μ the Lamé coefficients. The problem is to find u satisfying the three-dimensional scalar wave equation: $c^2 \nabla^2 u = \partial^2 u / \partial t^2$ with the sound speed $c = \sqrt{(\lambda + 2\mu) / \rho}$ where ρ is the density. The displacement field has a discontinuity across the crack surface $\Delta u(x, y, t) = u(x, y, 0^+, t) - u(x, y, 0^-, t)$, $\forall y < A(x, t)$. The stress must satisfy the boundary condition $\sigma = 0$ on the crack surface, i.e., $(\partial u / \partial z)(x, y, z = 0^\pm, t) = 0$ and meets the remote loading condition, i.e., the static external load.

The fracture energy G is the energy provided to the crack front by the flux of stored elastic energy per unit of new crack area. For small crack-front distortions, the energy release rate G can be expanded about a uniformly extending crack (RICE *et al.*, 1994; WILLIS and MOVCHAN, 1995; RAMANATHAN and FISHER, 1998) and specifically a first-order approximation can be used (SCHMITTBUHL and VILOTTE, 1999):

$$G(x) = G_0(1 + \mathcal{J}(x)) , \quad (1)$$

Where G_0 is the energy release rate for a quasi-static straight crack. The non-local kernel is given by (GAO and RICE, 1989):

$$\mathcal{J}(x, a(x, t)) = \frac{1}{\pi} PV \int_{-\infty}^{\infty} \frac{a(x') - a(x)}{(x - x')^2} dx' , \quad (2)$$

where PV is the principal value.

Accordingly the actual dynamics is replaced by the quasi-static approximation, i.e., elastic waves are neglected, and at each instant t the energy balance between mechanical energy and surface energy leads to:

$$G(x, t) = \Gamma(x, a(x, t)) . \quad (3)$$

5. Numerical Model

In order to characterize locally the heterogeneity of the interface, we introduce the fracture energy resistance $\Gamma(x, y)$ as a quenched disorder (i.e., a random fluctuation in space that does not evolve with time). To mimic the experiment, the fluctuations of the fracture energy resistance are assumed to be highly correlated over lengths smaller than a characteristic length d , and spatially uncorrelated at higher scales. The cut-off scale d has to be compared to the particle size of the sandblasting procedure ($d = 50 \mu\text{m}$). Accordingly, the interface is discretized into $N = L/d$ independent segments. The resistance is chosen for each segment from the definition: $\Gamma(x, y) = \Gamma_0[1 + \gamma(x, y)]$ where the average resistance Γ_0 is set to unity, and γ is obtained from a uniform distribution $[\gamma - \delta\gamma; \gamma + \delta\gamma]$.

To avoid edge effects, a L -periodic interface in the x direction is assumed such that the $1/x^2$ kernel in (2) transforms in $(\pi/L)^2 / \sin^2(\pi x/L)$ (GAO and RICE, 1989).

Loading results from an imposed displacement. An elementary step (i.e., a time step) corresponds to the motion of only one segment. At each step, the weakest segment is searched for (i.e., event driven dynamics) by assuming that its location x_w corresponds to the least fracture energy G_{\min} required to advance the crack SCHMITTBUHL *et al.*, 1995a; SCHMITTBUHL and VILOTTE, 1999):

$$G_{\min} = \Gamma_0 \min_{\forall x} \left[\frac{1 + \gamma(x, A(x, t))}{1 + \mathcal{F}(x, A(x, t))} \right] . \quad (4)$$

The most susceptible segment x_w is advanced by a fixed amount s that gives the unit length in the direction of propagation. At this stage, the crack is unloaded. The procedure is then repeated. The time scale is fixed by the updates of the weakest segments, and not directly related to the real time. After a transient regime, the system organizes into a statistically stationary state.

The behavior of the system is controlled by the competition between local fluctuations of the toughness and the effect of long-range elastic interactions. It can be shown (PERFETTINI *et al.*, 2001) that the stress drop of a point that just slipped by amount s is $2\mu s/(\pi d)$, where s is the slip size of elementary events and d is the discretization length. PERFETTINI *et al.* (2001) showed that the ratio of this stress drop and the rms of the toughness fluctuations $2\delta\gamma/\sqrt{12}$ defines the useful dimensionless parameter $\alpha = \mu s\sqrt{12}/(\pi d\delta\gamma)$. When α is much greater than unity ($\alpha \gg 1$), the elastic interactions screen the effect of the fluctuations of the toughness.

The heterogeneities are not strong enough to pin the front, thus crack advance can never be arrested. In our model under imposed displacement, the runaway of the crack is controlled from the imposed displacement, but this would not be the case with a model at fixed loading stress (see Fig. 8). This propagative regime will be denoted as regime **P**, and results in sidewise propagation of the crack.

When α is considerably smaller than unity ($\alpha \ll 1$), the heterogeneities of the toughness control the front advance (regime **SP** for strong pinning; see Fig. 8). This extreme regime may lead, for instance, to recurrent slip of the same segment, since the stress drop due to elastic interactions is not big enough (compared to $\delta\gamma$) to unload the point. For such a regime, the displacement field is expected to have the same statistical distribution as the fluctuations of the toughness, that is, a white noise in the present study.

For the intermediate regime, the magnitude of the elastic interactions is comparable to the amplitude of the toughness variations. This is a weak-pinning regime **WP** where the interactions between toughness heterogeneities and elastic stress transfers leads to nontrivial spatio-temporal correlations of slip (see Fig. 8) (SCHMITTBUHL *et al.*, 1995a; TANGUY *et al.*, 1998); SCHMITTBUHL and VILOTTE, 1999).

The simulations start with a zero displacement field. Figure 8 shows various slip distributions in steady state related to $\alpha = 10^{-4}$, 10^{-1} and 10^3 illustrating the three regimes mentioned above. We will focus on the intermediate regime **WP** ($\alpha \simeq 1$) where elastic interactions are comparable to variations of the toughness.

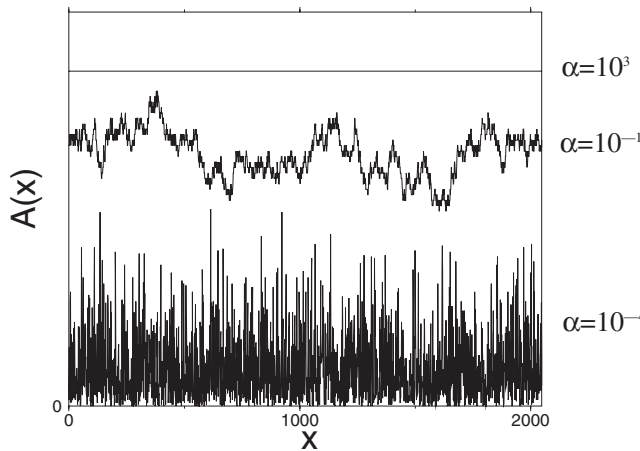


Figure 8

Sample of three fronts obtained from the numerical modeling for various α parameters. The x coordinate is in asperity size unit d . For $\alpha = 10^3$, elastic interactions dominate toughness fluctuations and the medium is seen as homogeneous. When $\alpha = 10^{-4}$, elastic coupling is negligible with respect to the influence of toughness fluctuations; roughness of the front is then controlled by the randomness of the toughness. For intermediate α ($\alpha = 10^{-1}$), the crack front develops spatial correlations over large distances.

6. Experiment and Model Comparison

In the numerical model, we let the front evolve from an initially flat slip with increasing displacement. After a transient regime, corresponding to the spreading of slip over the whole length of the sample, the slip correlations reach a stationary regime. The power spectrum (thin line) of the slip distribution, averaged over many fronts, is shown in Figure 9. On the same figure, the power spectrum related to the experimental results (heavy line) is also plotted. The power spectrum of the modeled front exhibits a power-law behavior, characteristics of self-affinity. The roughness exponent is found to be $\zeta \approx 0.35$, a value lower than the $\zeta \approx 0.6$ measured in our experiment.

Even though this model captures the main feature of the experimental observations i.e., the existence of a self-similar front, the value of the roughness exponent we obtain underestimates the value measured in the experiment. This difference in the value of the roughness exponent might come from:

1) *The influence of dynamical effects.* Using an experimental procedure similar to ours, MÅLØY and SCHMITTBUHL (2001) have studied the advance of a mode I crack (in-plane slip). They have observed that the front was advancing due to micro-

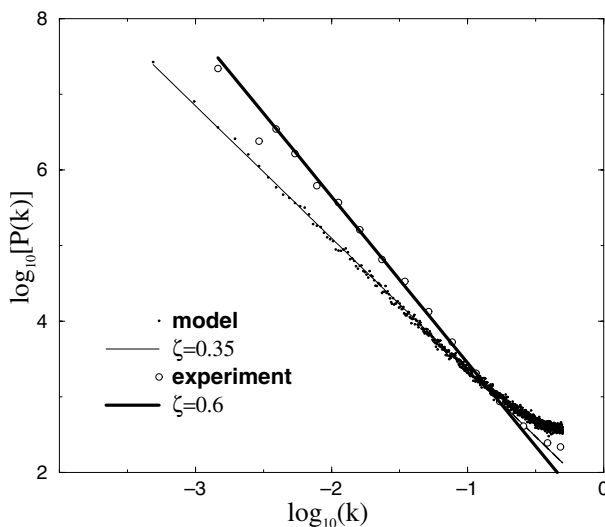


Figure 9

Comparison of the Power Spectra of experimental and numerical fronts. The wavelength unit is in pixel^{-1} (the pixel width is $2.6 \mu\text{m}$) for the experimental spectrum. For the numerical model, the unit of wave number is given by the size of the toughness fluctuation (i.e., the discretization size). Both spectra have a power-law behavior on a large range of scales, which shows the self-affine properties of the crack front roughness. However, slopes (that is, roughness exponents) are different: $\zeta \approx 0.35$ for the modeled fronts and $\zeta \approx 0.6$ for experimental fronts.

dynamic events associated with asperity depinning. This result suggests that the quasi-static approximation may be violated. Considering a complete elastodynamic description of this problem, RAMANATHAN and FISHER (1998) found a roughness exponent $\zeta \approx 0.5$, which is significantly higher than the value that is derived using a quasi-static approximation. This difference is very likely due to the presence of stress overshoots which are absent in our model.

2) *The existence of spatial correlations between toughness heterogeneities.* SCHMITTBUHL and VILOTTE (1999) have studied, using a model similar to ours, the influence of various types of these correlations (e.g., Gaussian-like). They showed that, although the self-affine behavior of the front was preserved, the value of the roughness exponent was affected by the presence of spatially correlated asperities. For a Gaussian spatial correlation of the toughness, the crack front shows a roughness exponent: $\zeta = 0.5$. The experimental roughness exponent $\zeta = 0.6$ can be obtained if the toughness fluctuations are spatially correlated using a power-law correlation function with an exponent of -0.4 .

3) *The influence of the process zone.* Due to the high stress ahead of the crack tip (crack theory predicts a $1/\sqrt{r}$ singularity, r being the distance from the crack tip), inelastic deformations and micro-fracture interactions may occur and modify locally the response of the medium. A more extended discussion of these type of effects can be found in BOUCHAUD (1997), LOPEZ and SCHMITTBUHL (1998), and ZAPPERI *et al.* (2000).

7. Crack Mode Analogies and Implications for Creeping Faults

The model described above assume a mode I crack. If a shear loaded half-plane crack, on the plane $z = 0$, is considered, it is commonly assumed that fracture processes under mixed mode loading are controlled by the energy release rate or the maximum shear intensity factor:

$$G = \frac{(1 - \nu)K_{II}^2 + K_{III}^2}{2\mu} \quad (5)$$

$$K = \sqrt{K_{II}^2 + K_{III}^2} \quad (6)$$

where ν and μ are respectively the Poisson's coefficient and the shear modulus of the elastic medium, while K_{II} and K_{III} are respectively the mode II and mode III stress intensity factors. For a strike-slip fault, concentration at the straight crack front is only controlled by the mode III loading, while for thrust or normal faults the mode II loading is dominant. GAO and RICE (1986) have derived the first-order perturbation of K_{II} and K_{III} for small deviations in the crack front geometry. This leads to a first-order coupling between mode II and mode III and therefore a second-order coupling effect in G or K . Following GAO *et al.* (1991), one may assume that in the first-order

analysis this coupling effect between the shear modes may be neglected, so that the perturbation in the local energy release rate may be written as:

$$G(x) = G^\infty \left(1 + \frac{M_\beta PV}{\pi} \int_{-\infty}^{\infty} \frac{a(x') - a(x)}{(x - x')^2} dx' \right), \quad (7)$$

where M_β is a constant depending on the shearing mode of loading, i.e., $\beta = \text{III}$ for mode III loading and $\beta = \text{II}$ for a mode II loading. This constant can be shown to depend only on the Poisson's coefficient ν with $M_{\text{II}} = (2 - 3\nu)/(2 - \nu)$ and $M_{\text{III}} = (2 + \nu)/(2 - \nu)$. Under this hypothesis, the non-local elastic interactions are of the same type as the model studied before, and our results can to some extent be relevant for mode II and mode III crack experiments.

Another interesting mathematical analogy can be noted here between the mode I perturbed crack front problem and the 2-D problem of an antiplane rupture along a frictional fault (GAO and RICE, 1989; PERRIN and RICE, 1994). In the antiplane rupture problem, the unbounded elastic medium contains a weak plane ($z = 0$) on which frictional sliding can occur. The elastic shear modulus is μ . Only displacement along the y direction is allowed and is presumed to be invariant in the y direction. This defines a model involving a single displacement variable u which satisfies a scalar wave equation and represents the shear slippage with the associated shear stress σ . The slip on the frictional plane is defined by the displacement discontinuity $\delta(x, t) = u(x, 0^+, t) - u(x, 0^-, t)$ and the shear stress is $\tau(x, t) = \sigma(x_1, 0, t)$. Frictional disorder on the fault, such as due to asperities, is introduced through a random pinning force $\eta_p(x, t)$. The quasistatic evolution of the antiplane shear rupture is actually governed by the same equations as the mode I crack problem, equations (1)–(3), provided the identification of the following variables:

$$\begin{cases} a(x, t) & \rightarrow & \delta(x, t) \\ \frac{G - G^\infty}{G^\infty} & \rightarrow & \frac{\tau}{2\mu} \\ \frac{\Gamma - G^\infty}{G^\infty} & \rightarrow & \frac{\eta_p - \tau^\infty}{2\mu} \end{cases}. \quad (8)$$

Since in the experiment the simulated fault is moving at a very slowly imposed rate, it is analogous to a creeping in-plane fault. If one accepts this analogy, our results have interesting implications for low-frequency slip inversions like GPS or InSar measurements, as pointed out by PERFETTINI *et al.* (2001). These instruments are low-pass filters, and will measure an important signal coming from slip on the fault, since the power spectrum of slip decreases with increasing wave number (see Fig. 9). However, the measured slip pattern will be smooth compared to the real one. This feature can be observed in Figure 10 where a synthetic front generated by the model (dark line) and the equivalent filtered one (grey line) are both plotted. The correlations of slip we observe in the experiments are clearly due to small-scale

asperities, however these scales are inaccessible to the latter instruments. Therefore, special care should be taken in the interpretation of areas of high slip measured by those instruments since they may not be due, in the view of the results of the experiment, to the presence of heterogeneities of the same size.

8. Conclusion

We have studied experimentally the slow propagation of an interfacial mode I crack in a transparent Plexiglas block. The crack advance has been shown to result from the depinning of asperities or micro-regions of high toughness. Self-affinity was observed, i.e., correlations of slip at all scales. The roughness exponent was found to be $\zeta \approx 0.63 \pm 0.05$. A quasi-static model was developed and was able to reproduce the self-similarity of the front with a roughness exponent $\zeta \approx 0.35$. The discrepancy between the observations and the model may be explained by dynamic effects (due to stress overshots), spatial correlations between asperities or non-elastic processes ahead of the crack tip. We have shown that the results, obtained in mode I, can easily be extended to mode II or III ruptures. These last two modes of rupture are relevant for the description of earthquakes where opening is unlikely to happen. Our results may have interesting applications to the interpretation of low-frequency data such as GPS or InSar.

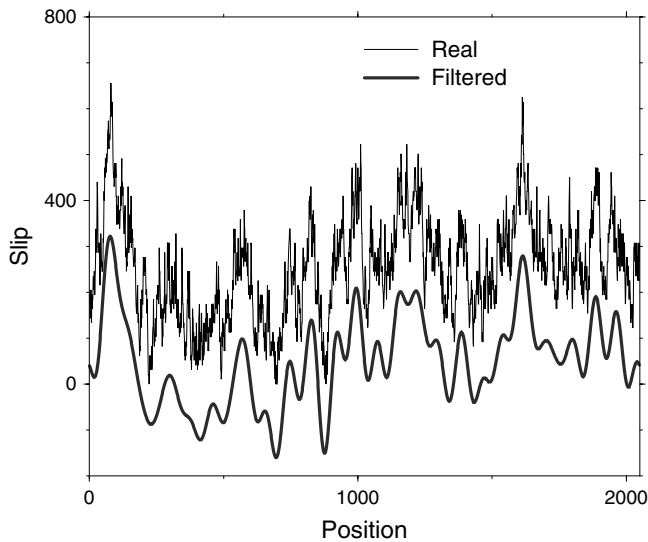


Figure 10

Comparison between the real and measured synthetic slip front of a creeping fault. Because of the low pass filter of the instrument (e.g., GPS or InSar), the small wavelengths are erased from the original signal.

From these results, the hypothesis that the average motion of a creeping fault may arise from a succession of micro-events related to breakage of asperities, is validated. In a mode I experiment similar to ours, MÅLØY and SCHMITTBUHL (2001) demonstrated that these micro-events were dynamical. This could help us view creeping faults differently. Even though these faults appear as moving continuously at large scale, the average slip may result from very localized dynamic instabilities or micro-earthquakes. Some of these events are often observed on creeping faults and one refers to them as micro-seismicity. However, it is possible that only the largest of these dynamic instabilities related to the depinning of large scale (of the order of many meters) asperities, are observed. Continuous slip may result from a series of dynamic events, where some, because of their significant size, are detected, while others, related to depinning of small asperities (such as the ones in the experiment), are beyond the detection threshold of seismic instruments. Such a speculative result, which needs further examination, has the advantage of collectively gathering seismically active and creeping faults, since slip on both of these faults would be due to dynamic instabilities.

Acknowledgements

This work was partially supported by ACI program “Risques Naturels” of the french educational minister and the CNRS program “Intérieur de la Terre.”

REFERENCES

- BOUCHAUD, E. (1997), *Scaling Properties of Cracks*, J. Phys.: Cond. Matter 9, 4319–4344.
- BOUCHAUD, E., LAPASSET, G., and PLANÈS, J. (1990), *Fractal Dimension of Fractured Surfaces: A Universal Value?*, Europhys. Lett. 13, 73–79.
- BOUCHAUD, J. P., BOUCHAUD, E., LAPASSET, G., and PLANÈS, J. (1993), *Models of Fractal Cracks*, Phys. Rev. Lett. 71, 2240.
- BROWN, S. R. and SCHOLZ, C. H. (1985), *Broad Bandwidth Study of the Topography of Natural Rock Surfaces*, J. Geophys. Res. 90, 12,575–12,582.
- COX, B. L. and WANG, J. S. Y. (1993), *Fractal Surfaces: Measurement and Application in Earth Sciences*, Fractals 1, 87–115.
- DELAPLACE, A., SCHMITTBUHL, J., and MÅLØY, K. (1999), *High Resolution Description of a Crack Front in an Heterogeneous Plexiglas Block*, Phys. Rev. E 60, 1337–1343.
- FISHER, D. (1998), *Collective Transport in Random Media: From Superconductors to Earthquakes*, Physics Reports 301, 113–150.
- GAO, H. and RICE, J. (1986), *Shear-stress Intensity Factors for a Planar Crack with Slightly Curved Front*, J. Appl. Mech. 53(4), 774–778.
- GAO, H. and RICE, J. R. (1989), *A First-order Perturbation Analysis of Crack Trapping by Arrays of Obstacles*, ASME J. Appl. Mech. 56, 828–836.
- GAO, H., RICE, J., and LEE, J. (1991), *Penetration of a Quasi-statically Slipping Crack into a Seismogenic Zone of Heterogeneous Fracture-resistance*, J. Geophys. Res. 96(B13), 21,535–21,548.
- LOPEZ, J. and SCHMITTBUHL, J. (1998), *Anomalous Scaling of Fracture Surfaces*, Phys. Rev. E 57, 6999–7005.

- MÅLØY, K. and SCHMITTBUHL, J. (2001), *Dynamical Instabilities during Slow Crack Propagation*, Phys. Rev. Lett. submitted.
- MÅLØY, K. J., HANSEN, A., HINRICHSEN, E. L., and ROUX, S. (1992), *Experimental Measurements of the Roughness of Brittle Cracks*, Phys. Rev. Lett. 68, 213–215.
- PERFETTINI, H., SCHMITTBUHL, J., and VILOTTE, J. (2001), *Slip Correlations on a Creeping Fault*, Geophys. Res. Lett. 28(10), 2133–2136.
- PERRIN, G. and RICE, J. N. (1994), *Disordering of Dynamic Planar Crack Front in a Model Elastic Medium of Randomly Variable Toughness*, J. Mech. Phys. Solids 42(6), 1047–1064.
- POWER, W. L., TULLIS, T. E., BROWN, S. R., BOITNOTT, G. N., and SCHOLZ, C. H. (1987), *Roughness of Natural Fault Surfaces*, Geophys. Res. Lett. 14, 29–32.
- RAMANATHAN, S. and FISHER, D. (1997), *Dynamics and Instabilities of Planar Tensile Cracks in Heterogeneous Media*, Phys. Rev. Lett. 79, 877–880.
- RAMANATHAN, S. and FISHER, D. (1998), *Onset of Propagation of Planar Cracks in Heterogeneous Media*, Phys. Rev. B 58, 6026–6046.
- RICE, J. R., BEN-ZION, Y., and KIM, K. (1994), *Three-dimensional Perturbation Solution for a Dynamic Planar Crack Moving Unsteadily in a Model Elastic Solid*, J. Mech. Phys. Solids 42, 813–843.
- SCHMITTBUHL, J. and MÅLØY, K. (1997), *Direct Observation of a Self-affine Crack Propagation*, Phys. Rev. Lett. 78, 3888–3891.
- SCHMITTBUHL, J. and VILOTTE, J. (1999), *Interfacial Crack Front Wandering: Influence of Correlated Quenched Noise*, Physica A 270, 42–56.
- SCHMITTBUHL, J., GENTIER, S., and ROUX, S. (1993), *Field Measurements of the Roughness of Fault Surfaces*, Geophys. Res. Lett. 20, 639–641.
- SCHMITTBUHL, J., ROUX, S., VILOTTE, J., and MÅLØY, K. (1995a), *Interfacial Crack Pinning: Effect of Non-local Interactions*, Phys. Rev. Lett. 74, 1787–1790.
- SCHMITTBUHL, J., SCHMITT, F., and SCHOLZ, C. (1995b), *Scaling Invariance of Crack Surfaces*, J. Geophys. Res. 100, 5953–5973.
- SCHMITTBUHL, J., VILOTTE, J., and ROUX, S. (1995c), *Reliability of Self-affine Measurements*, Phys. Rev. E 51, 131–147.
- SCHOLZ, C. H., *The Mechanics of Earthquakes and Faulting* (Cambridge Univ. Press, New York, 1990).
- SIMONSEN, I., HANSEN, A., and NES, O. M. (1998), *Using Wavelet Transforms for Hurst Exponent Determination*, Phys. Rev. E 58, 2779.
- TANGUY, A., GOUNELLE, M., and ROUX, S. (1998), *From Individual to Collective Pinning: Effect of Long-range Elastic Interactions*, Phys. Rev. E 58(2), 1577–1590.
- WILLIS, J. and MOVCHAN, A. (1995), *Dynamic Weight-functions for a Moving Crack: 1. Mode-I Loading*, J. Mech. Phys. Solids 43, 319–341.
- ZAPPERI, S., HERRMANN, H., and ROUX, S. (2000), *Planar Cracks in the Fuse Model*, Eur. Phys. J. B 17(1), 131–136.

(Received February 6, 2001, revised June 22, 2001, accepted August 1, 2001)



To access this journal online:
<http://www.birkhauser.ch>
